Selective Etching Induces Selective Growth and Controlled Formation of Various Platinum Nanostructures by Modifying Seed Surface Free Energy

Nini Fan, Yun Yang,* Wenfang Wang, Lijie Zhang, Wei Chen, Chao Zou, and Shaoming Huang*

Nanomaterials and Chemistry Key Laboratory, Wenzhou University, Wenzhou, Zhejiang 325027, People's Republic of China

ABSTRACT We present a strategy to achieve heterogeneous seeded growth on nanoparticle (NP) surfaces and construct various Pt nanostructures (cage- and ring-like) by using selective etching as surface-free-energy-distribution modifier. Preprepared Au polyhedron NPs (octahedron, decahedron, nanorod, and nanoplate) are mixed with KI, H_2PtCl_6, and surfactant. Under heating, KI is first oxidized to I_2, which then selectively etches the edges of Au polyhedrons. Consequently, the partial removal of surface Au atoms creates highly active sites (exposed high-index facets, atom steps, and kinks) on the etched edges. Then the reduced Pt^0 atoms deposit on the etched edges preferentially and grow further, generating bimetallic nanostructures, Au octahedrons, or decahedrons with edges coated by Pt. The Pt layer protects the Au on the etched edges against further etching, changing the etching route and causing the Au on {111} facets without a Pt layer to be etched. After the Au is removed completely from the bimetallic nanostructures, ring-like, frame-like, and octahedral cage-like Pt nanostructures form. The evolution from Au polyhedrons to Pt ring or octahedron cage is investigated systematically by high-resolution transmission electron microscopy, transmission electron microscopy, scanning electron microscopy, energy-dispersive X-ray, scanning transmission electron microscopy, and high-angle annular dark field.

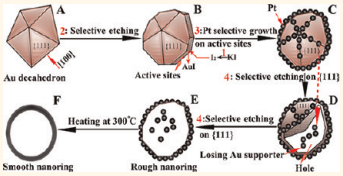

KEYWORDS: selective growth · selective etching · seeded growth · nanocage · nanoring

The controlled growth of noble nanostructures is a fascinating subject that has attracted much attention due to their promising applications in biosystem and catalysis.[1−12] Generally, the formation of NPs mainly includes two steps: nucleation, in which small-sized NPs form to serve as primary seeds, and consequent growth, in which later formed atoms deposit on the seeds' surface. In order to synthesize the nanostructures as designed, it is necessary to well control both nucleation and growth steps. During the past several decades, researchers have found that the complete separation of nucleation and growth, also named seeded growth, could offer them more power to tune the resulting nanostructures.[13−23] In the seeded growth, preprepared NPs act as nucleation centers, and other substances with the same or different chemical identity grow on their surface selectively. In general, if the seed and secondary substance have different chemical identity, the growth on the seed surface has two patterns according to the lattice mismatch degree: homogeneous seeded growth, in which the whole surface of the seeds acts as a nucleation site, and heterogeneous seeded growth, in which only part of the seed surface serves as a nucleation site.[24−44] For noble metals, due to their small lattice mismatch, the seeded growth employs a homogeneous pattern in most cases and the commonly formed structures are core@shell.[39] Several groups reported heterogeneous seeded growth and synthesized very interesting noble nanostructures successfully.[26,27,29,31,36] For example, Sun's group used Pt NPs as seeds and prepared Au-on-Pt hetero-oligomer NPs.[30] Xia and co-workers fabricated a dumbbell-like Pd−Au heterodimer by modifying overgrowth conditions.[31] Xu's group used the oil/water interface as reaction restrictor and synthesized a Au−Ag heterodimer.[26] In Mirkin's and Song's groups, Ag−Au−Ag segmented nanorods were synthesized, respectively.[29,36] In those reports, because of the system energy minimization trend, the growth mainly took place only on one facet of the seed and heterodimer or hetero-oligomer nanostructures formed. However so far, it is still a challenge to achieve selective growth only on specific positions of the seed surface, especially only on the edges or facets, and prepare NPs with edges or facets selectively coated by other substances. As far as we know, only Kitaev's and Torimoto's groups

* Address correspondence to bachier@163.com; smhuang@wzu.edu.cn.

Received for review February 1, 2012 and accepted April 13, 2012.

Published online April 13, 2012
10.1021/nn3004668

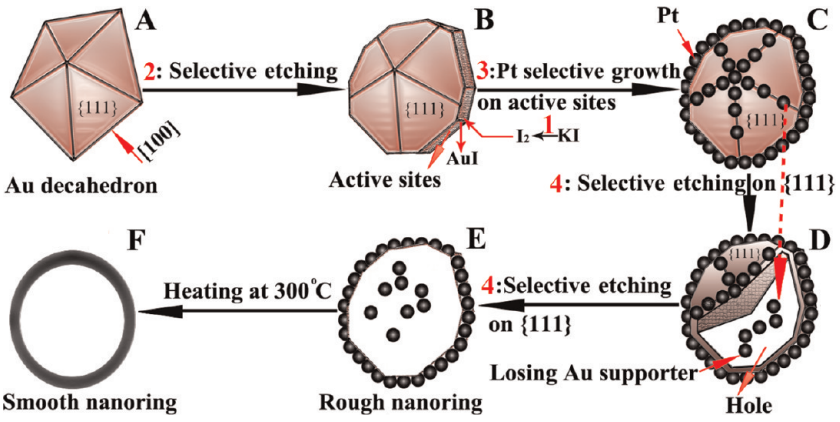

Figure 1. Schematic evolution from Au decahedron to Pt ring.

achieved such selective growth (Au on Ag NPs), and there are no similar reports between other metals.[45,46] This kind of selective growth is significant to the nanoscaled adjustments (structures and properties) and preparation of novel nanostructures.[45,46]

Here, we report a novel general method where selective etching is used to induce selective growth on crystal edges and generate a variety of Pt nanostructures (ring-, frame-, and cage-like). This method allows us to selectively grow Pt on the edges of Au polyhedrons capped by polymer.[48,49] In Kitaev's and Torimoto's strategies, selective growth on crystal edges was achieved by controlling the deposition rate and selectively capping the {100} facets, respectively.[45,46] As illustrated in Figure 1 and Figure S1, the key factor of our method is the selective etching along the crystal edges to create active sites (exposed high-index facets, defects, atom steps, and kinks)[50−56] by removing part of the surface atoms. The highly active sites act as nucleation sites and induce the selective deposition and growth of Pt on the etched edges, generating interesting bimetallic nanostructures (decahedral and octahedral Au NPs with edges coated by Pt). The Pt layer protects the Au on the etched edges against further etching. Subsequently, the Au on {111} facets that are free of Pt protection is removed completely, resulting in the formation of Pt nanorings and octahedral nanocages. Moreover, frame-like and hollow rod-like Pt nanostructures can also be generated through using Au nanoplates and nanorods as seeds, respectively. The following aspects in this paper are crucial. (I) The successful preparations of ring-, frame-, and cage-like Pt demonstrate that this method is a general route for selectively growing Pt on specific positions of Au NPs and preparing various Pt nanostructures. So far, hollow Pt structures can be prepared only through a galvanic reaction,[57−59] and there are reports on the frame-like Pt nanostructures. The strategy reported here provides another choice to generate hollow and other novel Pt nanostructures. (II) More importantly, selective etching driven by the inhomogeneous surface

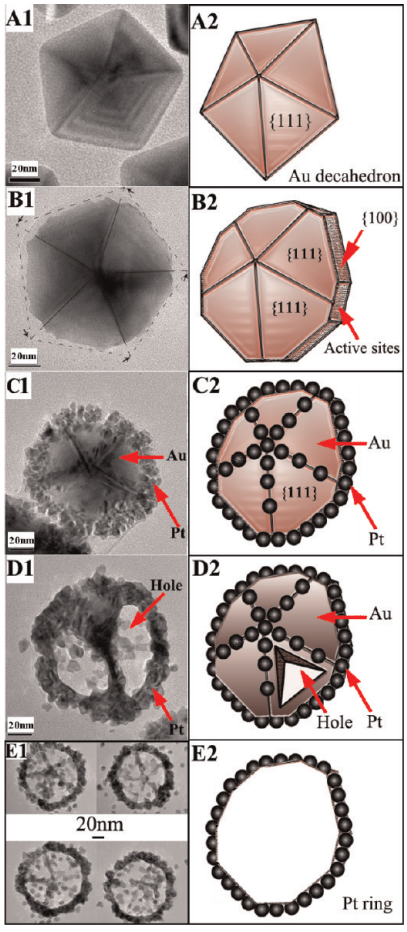

Figure 2. Typical TEM images and schematic diagrams of the NPs with different reaction times at 185 °C: (A) 0 min; (B) 40 min (dashed line: etched edge; solid line: unetched edge); (C) 50 min; (D) 60 min; (E) 70 min (Pt/Au = 0.5; 40 μL of 19 mM H_2PtCl_6).

free energy distribution of the NP surface exists among many substances. Thereby, this method could also be applied to non-noble nanostructures and impel researchers to construct interesting non-noble metal nanostructures. In addition, such cage-like nanostructures are promising drug carriers and could be applied in controlled drug release for disease therapy.[1,2,60]

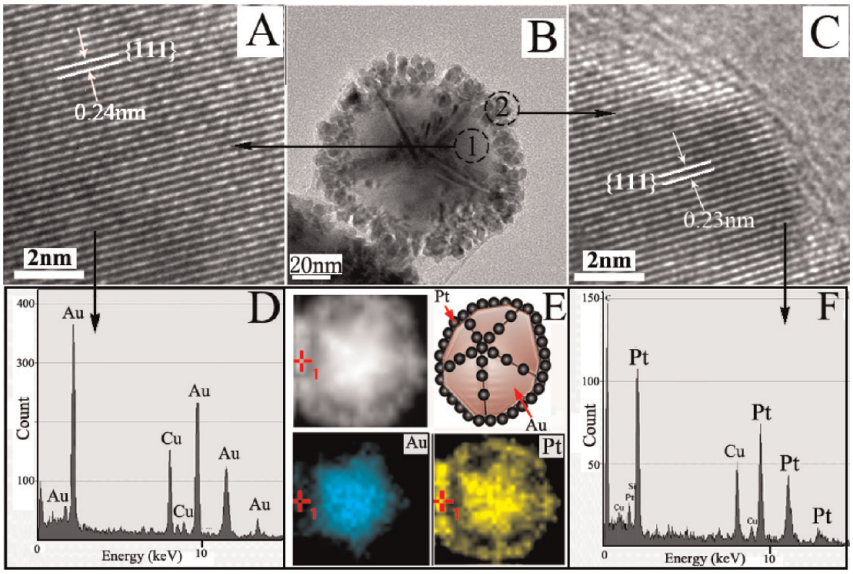

Figure 3. (A) HRTEM image of area 1 as indicated in (B); (B) TEM image of the NP; (C) HRTEM image of area 2 as indicated in (B); (D, F) EDS pattern of areas 1 and 2 (D for 1; F for 2); (E) STEM-EDS elemental mapping images and schematic diagram of one NP (green and yellow colors represent Au and Pt, respectively).

RESULTS AND DISCUSSION

In a typical synthesis, a solution containing Au decahedron seeds, KI (etchant precursor), polyvinylpyrrolidinone (PVP, MW = 58 000), and H_2PtCl_6 is heated at 185 °C in a sealed autoclave for different times. Detailed experiments can be found in the Supporting Information (SI). The decahedral Au seeds with smooth edges and {111} facets are shown in Figure 2A. After heating for 40 min, the edges of the Au NPs became rough owing to the etching (Figure 2B). Figure 2B1 shows that only the peripheral edges intersected by {111} and {100} facets were etched. However, the edges intersected by {111} facets have no distinct change. After etching, the Au decahedron lost five tips, marked by the arrows (Figure 2B1). When the reaction time was prolonged to 50 min, it was found that many small-sized NPs selectively grew on the etched edges (Figure 2C), and energy-dispersive X-ray (EDS) analysis reveals that they are Pt (Figure 3F). Meanwhile, small amounts of Pt NPs were also observed on the {111} facets and unetched edges. The analyses of high-resolution transmission electron microscopy (HRTEM), EDS, and scanning transmission electron microscopy (STEM-EDS) elemental mapping further confirm the selective growth of Pt on the etched edges (Figure 3A and C–F). The lattice distances in the {111} facet and the small NP are about 0.24 and 0.23 nm, respectively (Figure 3A and C), matching Au{111} and Pt{111}. The collected EDS signal from the {111} facet mainly belonged to Au element (Figure 3D) and that from the NPs on the etched edge chiefly to Pt element (Figure 3F), which agrees well with the HRTEM observations. The elemental mapping in Figure 3E gives the Pt and Au elemental distributions in one NP, which also demonstrates the selective growth of Pt on the etched edges. With the heating time increasing to 60 min, holes were visible on the {111} facet (Figure 2D), indicating that part of Au on the {111} facets was removed. After 70 min reaction, ring-like Pt nanostructures formed (Figure 2 E), indicating the Au decahedron seed was almost removed completely.

The scanning electron microscopy (SEM), STEM-EDS elemental mapping, HRTEM, and EDS analyses of the nanorings are shown in Figure 4 and Figure S5. The SEM image gives a clear ring-like view (Figure 4A). These ring-like nanostructures dominate the final product (Figure S5A), which demonstrates the high yield. It is noted that although most of the Au was removed, the nanorings still contain a small amount of Au (Figure 4B–D, Figure S5B). Probably, the residual Au was coated by Pt completely to form a core@shell structure and hence survived after the etching. The HRTEM image of the nanorings shows the interplane distance is about 0.23 nm (Figure 4E), which matches well with the {111} of Pt. The as-prepared nanorings are very rough (Figure 2E), but can become smooth after heating them at 300 °C for about 3 h under an Ar atmosphere because the small size effect results in a low melting point (Figure 4F and G).

When the octahedral Au NPs (Figure 5A) were used as seeds, similar selective etching and selective growth on etched edges were observed (Figures S1 and S6). However, the selective etching and selective growth happened on each edge of the Au octahedrons homogenously due to their same structure, which is different from the case of decahedral NPs, in which only the edges intersected by {111} and {100} were etched. After 70 min reaction, the final products were octahedral cage-like, which is demonstrated by the high-angle annular dark field (HAADF), TEM, HRTEM, and high-resolution SEM images (Figure 5B–F). The HRTEM image (Figure 5G) gives the interplane distance (0.199 nm),

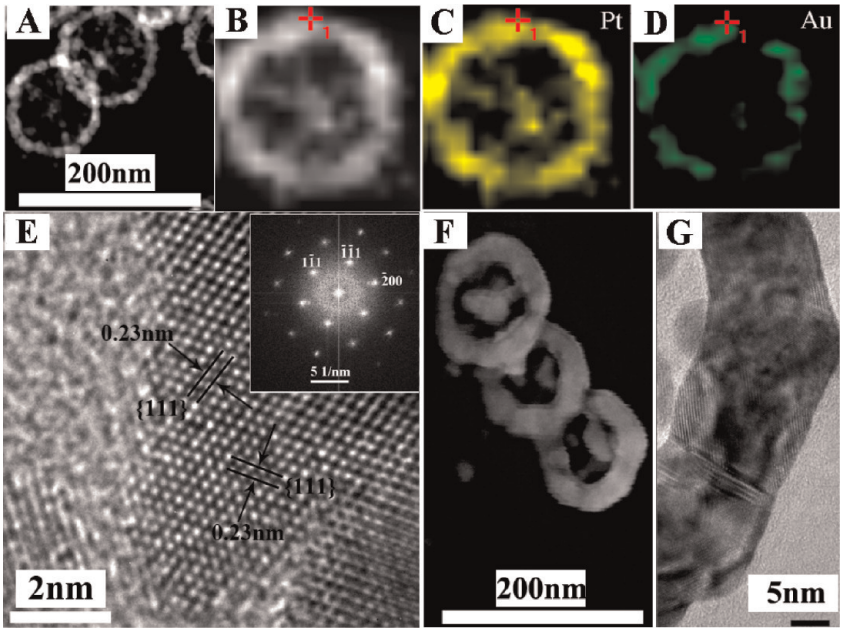

Figure 4. (A) SEM image of the nanorings; (B–D) HAADF and STEM-EDS elemental mapping images of one nanoring; (E) HRTEM image of the nanoring (inset is the fast Fourier transform pattern of the corresponding HRTEM image of (E), which demonstrates the crystalline feature); (F, G) SEM and HRTEM images of the nanoring prepared by heating the as-prepared rough ones at 300 °C (Pt/Au = 0.5, 40 μL of 19 mM H_2PtCl_6).

which is related with the {200} of Pt. The STEM-EDS elemental mapping (Figure 5H–I) and EDS pattern (Figure 5J) further reveal that the composition of the octahedral cage is Pt and the Au seeds were removed completely. It is worth nothing that not all octahedral cages have a perfect structure as depicted by Figure 5E. From the HRTEM image (Figure 5D), a Pt thin film also exists on the {111}. This is because the etching on {111} also could create highly active sites and a small amount of H_2PtCl_6 was still present at this stage. As a result, a small percentage of formed Pt atoms from the remaining precursor deposited on these active site of {111}, finally leading to formation of hollow octahedral Pt. By varying the used amount of H_2PtCl_6, the edge diameter of octahedral Pt nanocages can be tailored easily (Figure S11). It is worth noting that a molar ratio of Pt/Au less than 0.1 cannot form an intact octahedral Pt cage (Figure S11A), because the amount of Pt is not enough and the Pt NPs cannot interlink to preserve the structure of the octahedral template.

There is a distinct difference between the formation of octahedral Pt nanocages and that of nanorings. Many separated Pt NPs were observed during the formations of nanorings (Figure 2E); however no separated Pt NPs exist in the case of octahedral cages (Figure S6E). When the decahedral Au NPs acted as seeds, although Pt mainly grew on the etched edges, the growth of Pt on the unetched edges and {111} facets was also observed (Figure 2C and Figure 3E). However, because the amount of Pt on the unetched edges and facets is too small to interlink, it lost support and formed separated NPs after the Au seeds were removed. For the octahedral Au NP seeds, all edges were etched almost simultaneously and Pt NPs grew on each etched edge homogenously. Meanwhile, the Pt NPs interlinked through bonding, and thereby the octahedral cage-like structure could be preserved after the Au support was removed.

As presented in Figure 1 and Figure S1, it is believed that the evolution from Au polyhedrons to Pt nanocages and nanorings involves four main steps: (1) the *in situ* formation of I_2; (2) the selective etching along the edges of Au polyhedrons; (3) the reduction of Pt^{4+} to Pt^0 and the selective growth of Pt NPs on the etched edges of Au polyhedrons; (4) the change of selective etching route from along the edges to along the {111} facets of Au polyhedrons and the formation of Pt nanostructures (ring- and cage-like).

It is well known that Au^0 can be etched by KI/I_2 solution.[42] In our system, no I_2 was added, and it is believed that the I_2 in the etchant is from oxidized I^-. KI is an unstable substance and can be oxidized to I_2 easily by many oxidants especially under acidic or heating environment.[61,62] In our experiment, H_2PtCl_6 is an acid and the dissolved O_2 can act as an oxidant. Meanwhile, high temperature can accelerate the oxidization of I^- to I_2. In order to confirm this experimentally, a classic detection was performed. A colorless KI aqueous solution (Figure S12B) with the same 3.8 pH value as the solution for the preparation of the nanocage was sealed in an identical autoclave and heated at 185 °C. After 40 min, the colorless KI solution turned yellow (Figure S12C), and the KI/I_2 solution has a similar color (Figure S12A), indicating that I^- might be oxidized to I_2 by the dissolved O_2. The oxidization of I^- to I_2 was further confirmed by

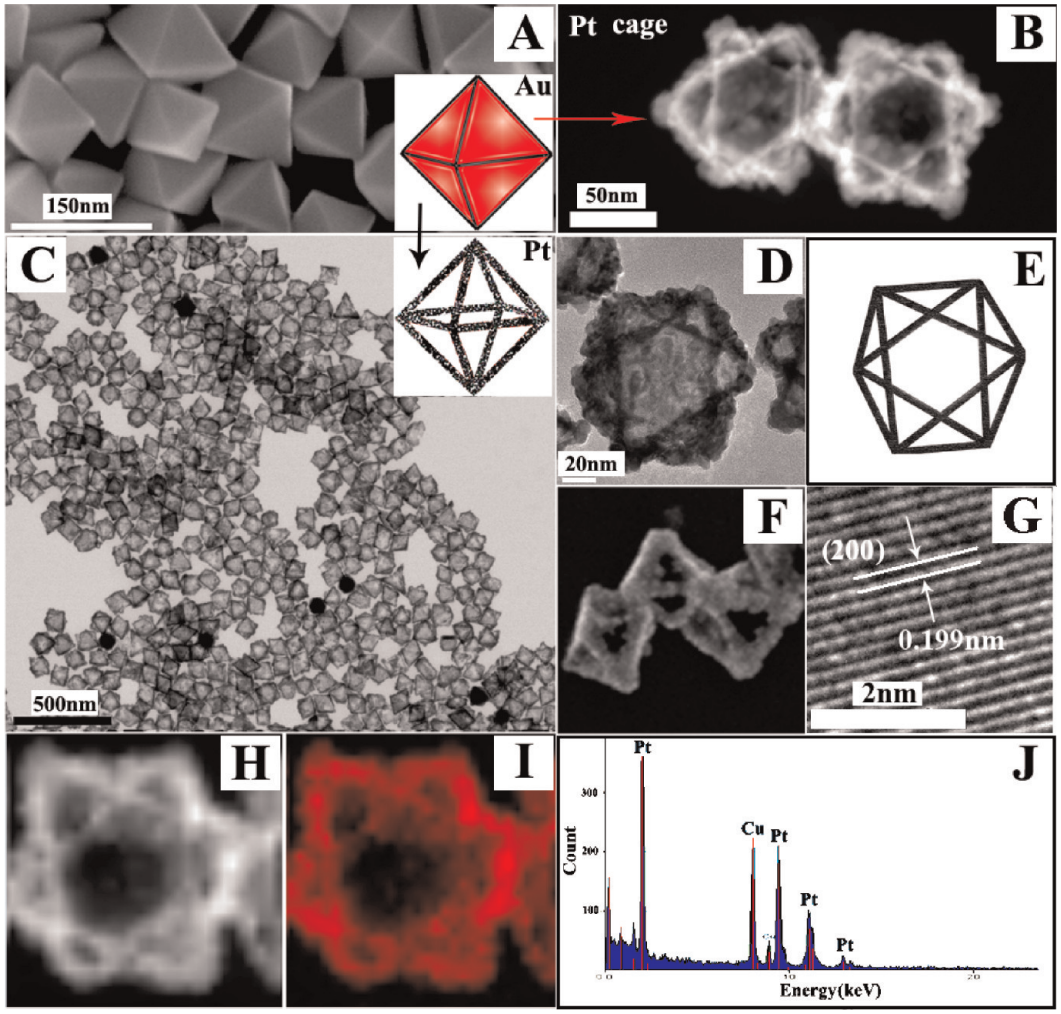

Figure 5. (A) SEM image of the Au octahedron seeds (inset is the geometric model); (B) HAADF image of the Pt cages; (C) TEM image of the Pt cages (inset is the geometric model) (Pt/Au = 0.2, 16 μL of 19 mM H_2PtCl_6); (D, E) HRTEM image and corresponding schematic image of the Pt cage; (F, G) SEM and HRTEM images of the Pt cages; (H, I) HAADF and STEM-EDS elemental mapping images of one Pt cage; (J) EDS pattern of the Pt cage shown in (H).

the classical chromogenic reaction between I_2 and starch (Figure S12D and E). In our system, H_2PtCl_6 is another oxidant for the oxidization of I^- to I_2. The oxidization of I^- by H_2PtCl_6 can be demonstrated by the reaction where I^- ions reduce Pt^{4+} to Pt^0 (Figure S16A).

In the second step, it is believed that the added KI together with the *in situ* formed I_2 is responsible for the selective etching along the edges of Au polyhedrons. Previously, Huang's group reported the etching of Au by O_2,[63] which means the etching of Au might be attributed to the dissolved O_2 instead of KI/I_2 in our system. In order to clarify this, a solution containing Au polyhedrons and PVP was heated at 185 °C for 1 h (no treatments were used to remove the dissolved O_2). Their UV−vis spectra and colors did not change (Figures S13 and S14), indicating that the Au NPs are unchanged and dissolved O_2 is unable to etch Au under our conditions. The etching of Au by KI/I_2 rather than O_2 can be demonstrated by another experiment. Under N_2 flow protection, after the Au colloid containing PVP, H_2PtCl_6, and KI was refluxed for 1 h, the redness and the characteristic UV−vis absorbance peak disappeared (Figure S15), implying that the Au NPs were etched and the absence of O_2 has no effect on the etching. In addition, we failed to prepare nanorings without KI (other conditions were unchanged) and even did not observe the etching of Au decahedrons (Figure 6), which also demonstrates that the etching resulted from KI/I_2.

It is commonly accepted that selective etching is caused by the inhomogeneous free energy distribution of the NP surface and the positions with high free energy are etched first.[64−70] In most cases, noble NPs are bound by three low-index facets ({111}, {100}, and {110}) and the energy rule is $E_{\{110\}} > E_{\{100\}} > E_{\{111\}}$.[64] Besides facets, another critical component of NP surfaces is crystal edge, which has a higher free energy than facets due to the existence of defects and strains.[71] Theoretically, the etching sequence should be from edge, to {110}, to {100}, to {111}. However, in practice, because surfactants or other substances adsorb preferentially on the specific positions of the NP surface, the surface free energy

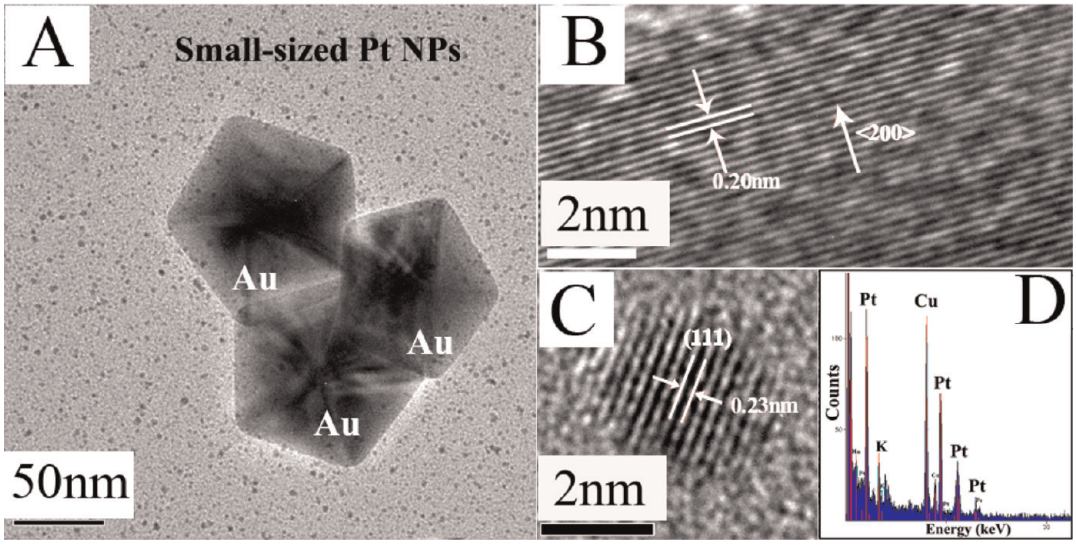

Figure 6. (A) TEM image of the NPs prepared without KI (185 °C; 70 min; Pt/Au = 0.2; 16 μL of 19 mM H_2PtCl_6); (B) HRTEM image of the Au decahedrons shown in (A); (C, D) HRTEM image and EDS pattern of the small-sized Pt NPs shown in (A).

distribution and selective etching direction can be changed.[66,71−76] For example, two groups respectively reported that the etching of octahedral 5NPs started from the tips along the [100] direction, although {100} is less active than {110}.[66,67] Xia's group demonstrated that the etching of decahedral Ag NPs started from the low-energy {111} facets due to the existence of O_2 at the edges.[71] Compared with the above previous studies, the etching of octahedral and decahedral Au NPs started from the edges in our experiment, which is reasonable energetically. In addition, the selective absorption of PVP molecules might also play an important role. During the formation process of octahedral and decahedral Au seeds, the {111}-terminated structure indicates that PVP molecules selectively adsorb on {111} and for this reason leave edges open to the etchant.[47−49] As a result, the edges with fewer stabilizers were etched first. Except for the above two causes, the strong binding interaction between I^- ions and the facet also should be considered. Generally, researchers argued that the I^- ion preferentially adsorbed on a specific facet of Au nanostructures in a given system.[77−79] For example, {111} is more attractive to I^- in solution containing CTAB.[77] However, the I^- ion has a stronger affinity with {110} and {100} than with {111} when the media contains PVP.[78] Our system involves using PVP as a capping agent and hence more possibly follows the latter. When KI was added in our experiment, I^- ions replaced the small number of PVP molecules which were absorbed on the edges due to their stronger affinity with Au than PVP (the prepared octahedron and decahedron nanoparticles have no perfect edges, and their edges more accurately should be small-area {100}).[79] Therefore, I_2 first formed in the edges, and reasonably the edges were etched preferentially.

The third step involves the reduction of Pt^{4+} to Pt^0 and the selective growth of Pt on the etched edges. It is believed that PVP and KI reduce Pt^{4+} to Pt^0 here. PVP always serves as a capping agent to prevent NPs from aggregating, and it also can be used as a reducing agent to prepare noble NPs.[80−82] KI also plays an important role in the reduction of Pt^{4+} to Pt^0 in our system. When H_2PtCl_6 solution containing KI or PVP was heated at 185 °C for 1 h, Pt NPs were clearly visible in two cases (Figure S16), indicating both KI and PVP can reduce Pt^{4+} to Pt^0. The reducing ability of PVP was also demonstrated by (Figure 6) small Pt NPs being present even though KI was not used.

As well as the selective etching, NP growth has strong dependence on the free energy distribution of the seed surface.[72] Generally, the positions with high surface free energy act as nucleation sites to induce selective growth along specific orientations, which leads to the formation of regularly shaped NPs.[47,83] In our experiment, selective growth means that the positions of the etched edges are more active than those of the unetched edges and facets. It was found that the selective growth of Pt did not happen in the absence of KI, and Pt separately nucleated to form small-sized Pt NPs (Figure 6), indicating the selective etching from iodide is crucial to the selective growth. That is to say, very likely the selective etching creates the active sites on the crystal edges through removing part of the surface Au atoms.[67,84] Han's group achieved the homogeneous seeded growth of Pt on polyhedral Au NP surface without etchant, also implying that selective etching is key to the selective growth.[85] In Figure 7A and B, an etched NP lies with a titled angle and its exposed {100} facets are very rough. Compared with smooth ones, the rough surfaces more likely have a high density of active sites (atom steps, defects, exposed high index facets, and kinks). The fine structure of the etched edge was observed *via* HRTEM (Figure 7C, D). The initial smooth edge became toothed due to the etching (Figure 7C). Distinctly, there is a high

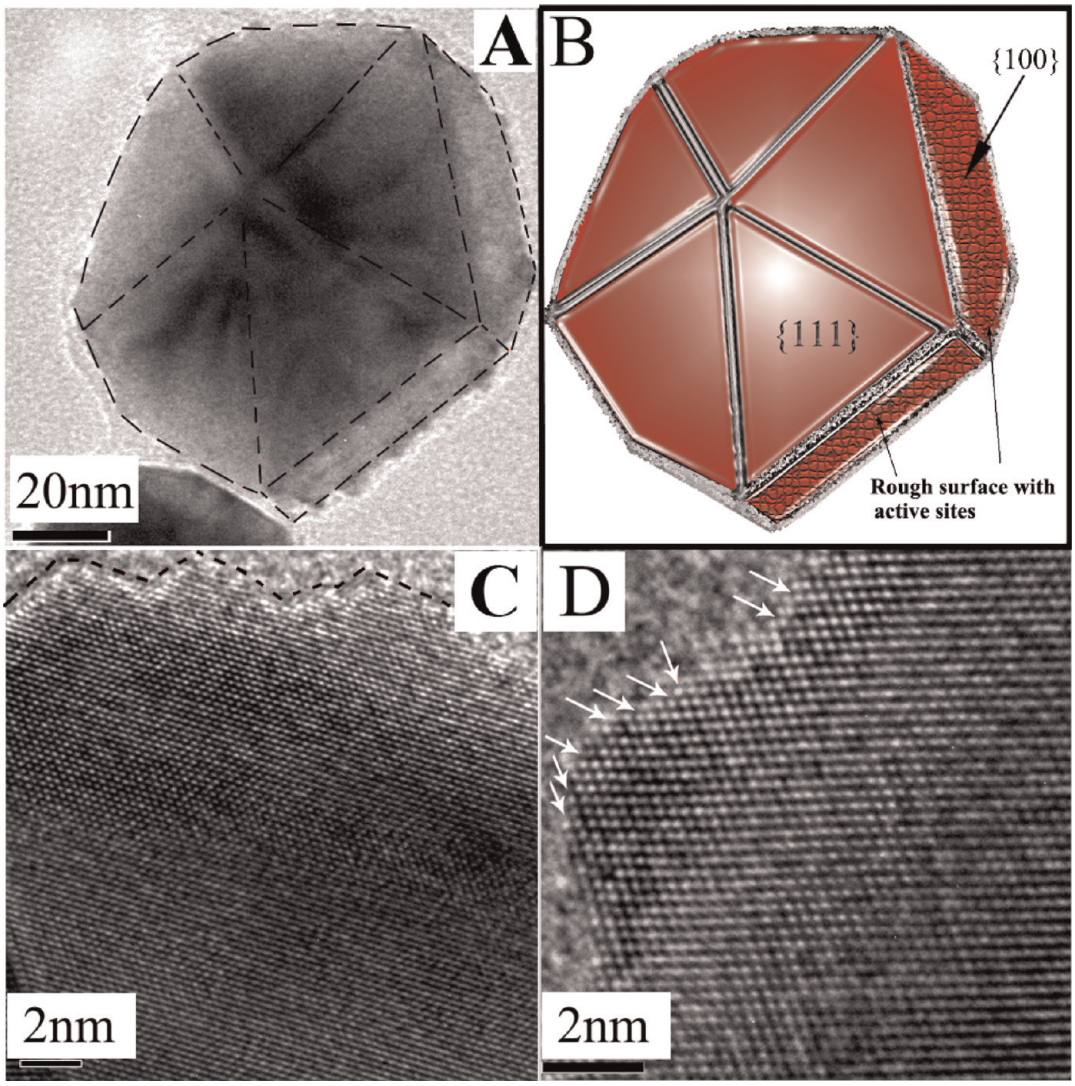

Figure 7. (A, B) TEM image and schematic diagram of one NP at 40 min reaction time at 185 °C (Initially, Au decahedron has no exposed {100} facets. The presence of {100} facets is due to the selective etching, which changes edges from line to face.) (C, D) HRTEM images of the rough etched edges (Pt/Au = 0.5; 40 μL of 19 mM H_2PtCl_6).

density of atom steps and exposed high index facets on the etched edges (Figure 7D), which demonstrates that the selective etching generates active nucleation sites and results in the selective growth on the edges.

The preferential adsorption of PVP on {111} facets also could make the edge accessible to the selective growth of Pt.[47,48] When our system was free of KI, selective growth was not observed even though PVP was used (Figure 6), demonstrating that the preferential adsorption of PVP on {111} facets is not responsible for the selective growth. Torimoto's group previously observed the selective growth of Au on the edges of thiol-capping Ag nanocubes.[46] However, in the case of PVP-capping Ag nanocubes, they did not observe such selective growth of Au on the edges, which is consistent with our observations.

According to the difference of antietching ability between Pt and Au, it is easy to explain the last step (the change of selective etching direction from the edges to the facets of Au polyhedrons and the formation of cage- and ring-like Pt nanostructures). Au can be etched by KI/I_2, but Pt has higher stability than Au and can resist the etching. After Pt deposited on the etched edges, the Pt coating layer protected the Au of these positions against further etching. Thus, KI/I_2 started etching the Au of {111} facets without Pt protection, finally leading to the formation of cage- and ring-like Pt nanostructures after the Au polyhedrons were removed.

During the preparation of decahedral Au NPs, a small amount of other shaped NPs (nanorods, triangular and hexagonal nanoplates) also formed. Compared with decahedral and octahedral Au, these NPs are bound by different facets (nanoplates by {110} and {111}; nanorods by {110}, {100}, and {111}).[86–88] After the selective etching and the selective growth were finished, triangular frames, hollow rods, and pentagonal frames formed (Figure 8). For nanoplates, the selective etching took place on the {110} facets first due to their high surface energy and created active sites there. As a result,

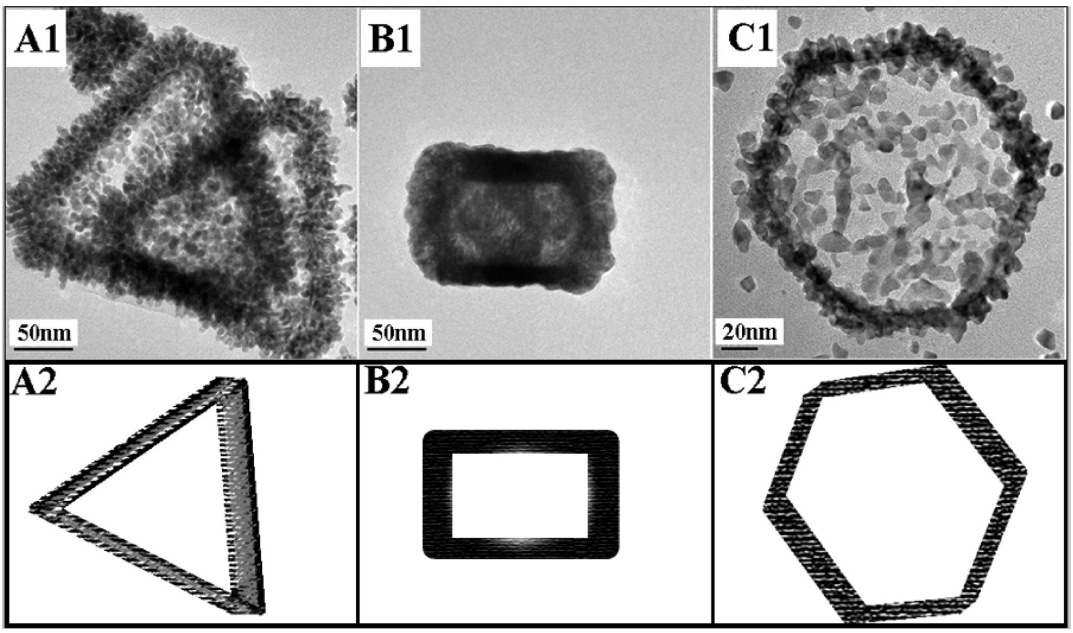

Figure 8. TEM images and sketches of other Pt nanostructures prepared using differently shaped Au NPs: (A) triangular frames; (B) hollow nanorod; (C) hexagonal frame (Pt/Au = 0.2; 16 μL of 19 mM H_2PtCl_6).

Pt selectively grew on the etched {110} facets, and subsequently the Au NPs of {111} facets were etched. Finally, triangular or hexagonal Pt frames formed. In the case of nanorods, generally a {111} facet exists on the two ends and the side facets are {100} and {110}.[87] Possibly, the initial etching occurred on {110} or {100} due to their high surface energy. Consequently, Pt atoms mostly grew on these positions, and the dark contrast confirms this result (Figure 8B1). The mechanism for the hollow rod is still not clear, and corresponding studies are being carried out *via* preparing Au nanorods on purpose. The formation of various Pt nanostructures (frame-, ring-, and cage-like) indicates that our strategy can be used as a general method to achieve the selective growth on specific positions (facet or edge) and build various Pt nanostructures. Au nanocrystals with a variety of shapes (cubes, concaved cubes, and hexagrams) could be prepared in high yield and their surfaces are bounded by different facets,[14,72,89] for example a cube by {100}, which could lead to different etching processes and formation of other structured Pt. Next, we will try to prepare variously shaped Au nanocrystals, and systematic studies of shape-dependent etching will be carried out.

SUMMARY

We have demonstrated that selective etching can be used as a general way to achieve selective growth on specific positions (facet or edge) and construct various Pt nanostructures (octahedral cages, nanorings, hollow rods, triangular and hexagonal frames). The selective etching by I_2 formed *in situ* from the reduction of the added KI is demonstrated to be the key factor. The selective etching preferentially created highly active sites on the crystal edges or facets, which served as nucleation sites to direct the selective deposition and growth of Pt along them. The Pt coating layer protected the Au on etched positions against further etching, changing the etching direction and causing the Au of the {111} facet without Pt protection to be etched. Finally, ring-like, cage-like, frame-like, and hollow rod-like Pt nanostructures could be fabricated after the Au seeds were removed completely. Because selective etching driven by the inhomogeneous free energy distribution of the NP surface exists among many substances, this method reported here could be a general route to fabricate both noble and non-noble metal nanostructures. Furthermore, the prepared Pt-based nanostructures can also serve as catalysts for fuel cells, drug carriers for medical applications, and template for generating other functional materials with similar structures as well. More studies are under way to further explore their potential applications.

METHODS

Chemicals. $HAuCl_4$, ethylene glycol (EG), diethylene glycol (DEG), PVP, poly(diallyldimethylammonium chloride) (PDDA, M_w = 400 000–500 000, 20 wt % in H_2O), KI, and H_2PtCl_6 were purchased from Aldrich and used as received without further purifications.

Synthesis of Octahedral Au NPs. The synthesis of Au octahedra followed a method reported by Cho's group.[49] Typically, 80 mL of EG was mixed with 1.6 mL of PDDA under stirring, and then 20 mg of $HAuCl_4$ was added to form a yellow solution. The resulting yellow solution was put into a 195 °C oil bath. After 30 min, the

heating source was removed and the obtained red colloid was cooled to room temperature. In order to remove excess PDDA and EG, 80 mL of water was introduced into the above colloid, and then it was centrifuged (12 000 rpm) for 15 min. The collected NPs were dispersed in water and centrifuged again. The purification was repeated three times, and the resulting NPs were dissolved in 60 mL of water for further applications.

Preparation of Decahedral Au NPs. A method developed by Song's group was used to prepare Au decahedron NPs.[47,48] In a typical preparation, 5 g of PVP was dissolved in 25 mL of DEG, and the solution was heated to boiling. Then 2 mL of another DEG containing 20 mg of $HAuCl_4$ was injected quickly into the boiling solution. Immediately, the solution changed from colorless to red. After 10 min of refluxing, it was cooled to room temperature and a similar purifying process to the above octahedral NPs was employed to remove excess PVP and DEG.

Preparations of Various Pt Nanostructures. A 2 mL amount of purified colloid was mixed with 10 mg of PVP, a calculated amount of 19 mM H_2PtCl_6 (8 μL, Pt/Au = 0.1; 16 μL, Pt/Au = 0.2; 24 μL, Pt/Au = 0.3; 40 μL, Pt/Au = 0.5), and 2 mg of KI. Then 3 mL of water was added. The mixture was sealed in a 20 mL autoclave and heated at 185 °C for different times. After the reaction was finished, the obtained colloid was washed through similar purification to the above octahedral NPs except that the centrifuge speed was 8000 rpm.

Characterizations. For TEM, HRTEM, EDS, HAADF, and STEM-EDS, corresponding purified colloids were deposited on copper grids coated by a carbon membrane and dried at 80 °C. After the water was removed completely, the sample was observed on a 300KV Tecnai G2 F30 S-Twin microscope with an attached EDS. For SEM, a similar preparation of the sample was used except that a Si wafer was used as sample support. The UV–vis spectra of NP colloids were recorded by a Shimadzu 2450 UV–vis spectrophotometer at room temperature.

Conflict of Interest: The authors declare no competing financial interest.

Acknowledgment. This work was supported by the NSFC (21101120, 21173159, 51025207), ZJST (2010C31039), ZJNSF (Y4110391, R4090137), and LCST (T100106).

Supporting Information Available: Other TEM, EDS, and HRTEM results are included. This material is available free of charge *via* the Internet at http://pubs.acs.org.

REFERENCES AND NOTES

1. Moon, G.; Choi, S.; Cai, X.; Li, W.; Cho, E.; Jeong, U.; Wang, L.; Xia, Y. A New Theranostic System Based on Gold Nanocages and Phase-Change Materials with Unique Features for Photoacoustic Imaging and Controlled Release. *J. Am. Chem. Soc.* **2011**, *133*, 4762–4765.
2. Chen, J.; Wang, D.; Xi, J.; Au, L.; Siekkinen, A.; Warsen, A.; Li, Z.; Zhang, H.; Xia, Y.; Li, X. Immuno Gold Nanocages with Tailored Optical Properties for Targeted Photothermal Destruction of Cancer Cells. *Nano Lett.* **2007**, *7*, 1318–1322.
3. Xu, C.; Xie, J.; Ho, D.; Wang, C.; Kohler, N.; Walsh, E. G.; Morgan, J. R.; Chin, Y. E.; Sun, S. Au-Fe_3O_4 Dumbbell Nanoparticles as Dual Functional Probes. *Angew. Chem., Int. Ed.* **2008**, *47*, 173–176.
4. Murphy, C. J.; Gole, A. M.; Stone, J. W.; Sisco, P. N.; Alkilani, A. M.; Goldsmith, E. C.; Baxter, S. C. Gold Nanoparticles in Biology: Beyond Toxicity to Cellular Imaging. *Acc. Chem. Res.* **2008**, *41*, 1721–1730.
5. Jana, N. R.; Ying, J. Y. Synthesis of Functionalized Au Nanoparticles for Protein Detection. *Adv. Mater.* **2008**, *20*, 430–434.
6. Giljohann, D.; Seferos, D.; Daniel, W.; Massich, M.; Patel, P.; Mirkin, C. Gold Nanoparticles for Biology and Medicine. *Angew. Chem., Int. Ed.* **2010**, *49*, 3280–3294.
7. Lee, H.; Habas, S. E.; Somorjai, G. A.; Yang, P. Localized Pd Overgrowth on Cubic Pt Nanocrystals for Enhanced Electrocatalytic Oxidation of Formic Acid. *J. Am. Chem. Soc.* **2008**, *130*, 5406–5407.
8. Narayanan, R.; El-Sayed, M. A. Effect of Catalysis on the Stability of Metallic Nanoparticles: Suzuki Reaction Catalyzed by PVP-Palladium Nanoparticles. *J. Am. Chem. Soc.* **2003**, *125*, 8340–8347.
9. Joo, S.; Park, J.; Tsung, C.; Yamada, Y.; Yang, P.; Somorjai, G. A. Thermally Stable Pt/mesoporous Silica Core–Shell Nanocatalysts for High-Temperature Reactions. *Nat. Mater.* **2009**, *8*, 126–131.
10. Jang, Y.; Kim, S.; Jun, S.; Kim, B.; Hwang, S.; Song, I.; Kim, M.; Hyeon, T. Simple One-Pot Synthesis of Rh-Fe_3O_4 Heterodimer Nanocrystals and Their Applications to a Magnetically Recyclable Catalyst for Efficient and Selective Reduction of Nitroarenes and Alkenes. *Chem. Commun.* **2011**, *47*, 3601–3603.
11. Wang, C.; Daimon, H.; Lee, Y.; Kim, J.; Sun, S. Synthesis of Monodisperse Pt Nanocubes and Their Enhanced Catalysis for Oxygen Reduction. *J. Am. Chem. Soc.* **2007**, *129*, 6974–6975.
12. Peng, Z.; You, H.; Yang, H. An Electrochemical Approach to PtAg Alloy Nanostructures Rich in Pt at the Surface. *Adv. Funct. Mater.* **2010**, *20*, 3734–3741.
13. Yu, Y.; Zhang, Q.; Lu, X.; Lee, J. Seed-Mediated Synthesis of Monodisperse Concave Trisoctahedral Gold Nanocrystals with Controllable Sizes. *J. Phys. Chem. C* **2010**, *114*, 11119–11126.
14. Sau, T.; Murphy, C. Room Temperature, High-Yield Synthesis of Multiple Shapes of Gold Nanoparticles in Aqueous Solution. *J. Am. Chem. Soc.* **2004**, *126*, 8648–8649.
15. Wang, F.; Li, C.; Sun, L.; Wu, H.; Ming, T.; Wang, J.; Yu, J.; Yan, C. Heteroepitaxial Growth of High-Index-Faceted Palladium Nanoshells and Their Catalytic Performance. *J. Am. Chem. Soc.* **2011**, *133*, 1106–1111.
16. Huang, X.; Tang, S.; Mu, X.; Dai, Y.; Chen, G.; Zhou, Z.; Yang, Z.; Zheng, N. Freestanding Palladium Nanosheets with Plasmonic and Catalytic Properties. *Nat. Nanotechnol.* **2011**, *6*, 28–32.
17. Fan, F.; Liu, D.; Wu, Y.; Duan, S.; Xie, Z.; Jiang, Z.; Tian, Z. Epitaxial Growth of Heterogeneous Metal Nanocrystals: From Gold Nano-octahedra to Palladium and Silver Nanocubes. *J. Am. Chem. Soc.* **2008**, *130*, 6949–6951.
18. Chen, W.; Yu, R.; Li, L.; Wang, A.; Peng, Q.; Li, Y. A Seed-Based Diffusion Route to Monodisperse Intermetallic CuAu Nanocrystals. *Angew. Chem., Int. Ed.* **2010**, *49*, 2917–2921.
19. Sánchez-Iglesias, A.; Carbó-Argibay, E.; Glaria, A.; Rodríguez-González, B.; Pérez-Juste, J.; Pastoriza-Santos, I.; Liz-Marzán, L. M. Rapid Epitaxial Growth of Ag on Au Nanoparticles: From Au Nanorods to Core-Shell Au@Ag Octahedrons. *Chem.—Eur. J.* **2010**, *16*, 5558–5563.
20. Pazos-Prez, N.; Barbosa, S.; Rodríguez-Lorenzo, L.; Aldeanueva-Potel, P.; Pérez-Juste, J.; Pastoriza-Santos, I.; Alvarez-Puebla, R.; Liz-Marzán, L. Growth of Sharp Tips on Gold Nanowires Leads to Increased Surface-Enhanced Raman Scattering Activity. *J. Phys. Chem. Lett.* **2010**, *1*, 24–27.
21. Ma, Y.; Li, W.; Cho, E.; Li, Z.; Yu, T.; Zeng, J.; Xie, Z.; Xia, Y. Au@Ag Core-Shell Nanocubes with Finely Tuned and Well-Controlled Sizes, Shell Thicknesses, and Optical Properties. *ACS Nano* **2010**, *4*, 6725–6734.
22. Wang, L.; Yamauchi, Y. Strategic Synthesis of Trimetallic Au@Pd@Pt Core-Shell Nanoparticles from Poly(vinylpyrrolidone)-Based Aqueous Solution toward Highly Active Electrocatalysts. *Chem. Mater.* **2011**, *23*, 2457–2465.
23. Habas, S.; Lee, H.; Radmilovic, V.; Somorjai, G. A.; Yang, P. Shaping Binary Metal Nanocrystals through Epitaxial Seeded Growth. *Nat. Mater.* **2007**, *6*, 692–697.
24. Carbone, L.; Cozzoli, P. Colloidal Heterostructured Nanocrystals: Synthesis and Growth Mechanisms. *Nano Today* **2010**, *5*, 449–493.
25. Zhang, J.; Tang, Y.; Lee, K.; Ouyang, M. Nonepitaxial Growth of Hybrid Core-Shell Nanostructures with Large Lattice Mismatches. *Science* **2010**, *327*, 1634–1638.
26. Gu, H.; Yang, Z.; Gao, J.; Chang, K.; Xu, B. Heterodimers of Nanoparticles: Formation at a Liquid–Liquid Interface and Particle-Specific Surface Modification by Functional Molecules. *J. Am. Chem. Soc.* **2005**, *127*, 34–35.
27. Park, K.; Vaia, R. Synthesis of Complex Au/Ag Nanorods by Controlled Overgrowth. *Adv. Mater.* **2008**, *20*, 3882–3886.

28. Lim, B.; Jiang, M.; Camargo, P.; Cho, E.; Tao, J.; Lu, X.; Zhu, Y.; Xia, Y. Pd-Pt Bimetallic Nanodendrites with High Activity for Oxygen Reduction. *Science* **2009**, *324*, 1302–1305.
29. Seo, D.; Yoo, C.; Jung., J.; Song, H. Ag−Au−Ag Heterometallic Nanorods Formed through Directed Anisotropic Growth. *J. Am. Chem. Soc.* **2008**, *130*, 2940–2941.
30. Wang, C.; Tian, W.; Ding, Y.; Ma, Y.; Wang, Z.; Markovic, N.; Stamenkovic, V.; Daimon, H.; Sun, S. Rational Synthesis of Heterostructured Nanoparticles with Morphology Control. *J. Am. Chem. Soc.* **2010**, *132*, 6524–6529.
31. Lim, B.; Kobayashi, H.; Yu, T.; Wang, J.; Kim, M.; Li, Z.; Rycenga, M.; Xia, Y. N. Synthesis of Pd−Au Bimetallic Nanocrystals *via* Controlled Overgrowth. *J. Am. Chem. Soc.* **2010**, *132*, 2506–2507.
32. Grzelczak, M.; Pérez-Juste, J.; Mulvaney, P.; Liz-Marzán, L. Shape Control in Gold Nanoparticle Synthesis. *Chem. Soc. Rev.* **2008**, *37*, 1783–1791.
33. Gou, L.; Murphy, C. Fine-Tuning the Shape of Gold Nanorods. *Chem. Mater.* **2005**, *17*, 3668–3672.
34. Mokari, T.; Sztrum, C.; Salant, A.; Rabani, E.; Banin, U. Formation of Asymmetric One-Sided Metal-Tipped Semiconductor Nanocrystal Dots and Rods. *Nat. Mater.* **2005**, *4*, 855–863.
35. Vaneski, A.; Susha, A.; Rodríguez-Fernández, J.; Berr, M.; Jäckel, F.; Feldmann, J.; Rogach, A. Hybrid Colloidal Heterostructures of Anisotropic Semiconductor Nanocrystals Decorated with Noble Metals: Synthesis and Function. *Adv. Mater.* **2011**, *21*, 1547–1556.
36. Langille, M.; Zhang, J.; Mirkin, C. A. Plasmon-Mediated Synthesis of Heterometallic Nanorods and Icosahedra. *Angew. Chem., Int. Ed.* **2011**, *50*, 3543–3547.
37. Wang, A.; Peng, Q.; Li, Y. Rod-Shaped Au−Pd Core−Shell Nanostructures. *Chem. Mater.* **2011**, *23*, 3217–3222.
38. Zhang, H.; Jin, M.; Wang, J.; Kim, M.; Yang, D.; Xia, Y. Synthesis of Pd−Pt Bimetallic Nanocrystals with a Concave Structure through a Bromide-Induced Galvanic Replacement Reaction. *J. Am. Chem. Soc.* **2011**, *133*, 6078–6089.
39. Wang, F.; Sun, L.; Feng, W.; Chen, H.; Yeung, M.; Wang, J.; Yan, C. Heteroepitaxial Growth of Core-Shell and Core-Multishell Nanocrystals Composed of Palladium and Gold. *Small* **2010**, *6*, 2566–2575.
40. Niu, W.; Zheng, S.; Wang, D.; Liu, X.; Li, H.; Han, S.; Chen, J.; Tang, Z.; Xu, G. Selective Synthesis of Single-Crystalline Rhombic Dodecahedral, Octahedral, and Cubic Gold Nanocrystals. *J. Am. Chem. Soc.* **2009**, *131*, 697–703.
41. Zhang, K.; Xiang, Y.; Wu, X.; Feng, L.; He, W.; Liu, J.; Zhou, W.; Xie, S. Enhanced Optical Responses of Au@Pd Core/Shell Nanobars. *Langmuir* **2009**, *25*, 1162–1168.
42. Lee, Y.; Carcia, M.; Frey Huls, N.; Sun, S. Synthetic Tuning of the Catalytic Properties of $AuFe_3O_4$ Nanoparticles. *Angew. Chem., Int. Ed.* **2010**, *49*, 1271–1274.
43. Jana, N.; Peng, X. Single-Phase and Gram-Scale Routes toward Nearly Monodisperse Au and Other Noble Metal Nanocrystals. *J. Am. Chem. Soc.* **2003**, *125*, 14280–14281.
44. Yang, J.; Ying, J. A General Phase-Transfer Protocol for Metal Ions and Its Application in Nanocrystal Synthesis. *Nat. Mater.* **2009**, *8*, 683–689.
45. McEachran, M.; Keogh, D.; Pietrobon, B.; Cathcart, N.; Gourevich, I.; Coombs, N.; Kitaev, V. Ultrathin Gold Nanoframes through Surfactant-Free Templating of Faceted Pentagonal Silver Nanoparticles. *J. Am. Chem. Soc.* **2011**, *133*, 8066–8069.
46. Okazaki, K.; Yasui, J.; Torimoto, T. Electrochemical Deposition of Gold Frame Structure on Silver Nanocubes. *Chem. Commun.* **2009**, 2917–2919.
47. Seo, D.; Yoo, C; Chung, I.; Park, S.; Ryu, S.; Song, H. Shape Adjustment between Multiply Twinned and Single-Crystalline Polyhedral Gold Nanocrystals: Decahedra, Icosahedra, and Truncated Tetrahedra. *J. Phys. Chem. C* **2008**, *112*, 2469–2475.
48. Seo, D.; Park, J.; Jung, J.; Park, S.; Ryu, S.; Kwak, J.; Song, H. One-Dimensional Gold Nanostructures through Directed Anisotropic Overgrowth from Gold Decahedrons. *J. Phys. Chem. C* **2009**, *113*, 3449–3454.
49. Li, C.; Shuford, K.; Chen, M.; Lee, E.; Cho, S. A Facile Polyol Route to Uniform Gold Octahedra with Tailorable Size and Their Optical Properties. *ACS Nano* **2008**, *2*, 1760–1769.
50. Yu, T.; Kim, D.; Zhang, H.; Xia, Y. Platinum Concave Nanocubes with High-Index Facets and Their Enhanced Activity for Oxygen Reduction Reaction. *Angew. Chem., Int. Ed.* **2011**, *50*, 2773–2777.
51. Huang, X.; Zhao, Z.; Fan, J.; Tan, Y.; Zheng, N. Amine-Assisted Synthesis of Concave Polyhedral Platinum Nanocrystals Having {411} High-Index Facets. *J. Am. Chem. Soc.* **2011**, *133*, 4718–4721.
52. Zhou, Z.; Tian, N.; Huang, Z.; Chen, D.; Sun, S. Nanoparticle Catalysts with High Energy Surfaces and Enhanced Activity Synthesized by Electrochemical Method. *Faraday Discuss.* **2008**, *140*, 81–92.
53. Tian, N.; Zhou, Z.; Sun, S.; Ding, Y.; Wang, Z. Synthesis of Tetrahexahedral Platinum Nanocrystals with High-Index Facets and High Electro-Oxidation Activity. *Science* **2007**, *316*, 732–735.
54. Zheng, Y.; Tao, J.; Liu, H.; Zeng, J.; Yu, T.; Ma, Y.; Moran, C.; Wu, L.; Zhu, Y.; Liu, J.; Xia, Y. Facile Synthesis of Gold Nanorice Enclosed by High-Index Facets and Their Application for CO Oxidation. *Small* **2011**, *7*, 2307–2312.
55. Watt, J.; Cheong, S.; Toney, M.; Ingham, B.; Cookson, J.; Bishop, P.; Tilley, R. Ultrafast Growth of Highly Branched Palladium Nanostructures for Catalysis. *ACS Nano* **2010**, *4*, 396–402.
56. Guo, S.; Li, J.; Dong, S.; Wang, E. Three-Dimensional Pt-on-Au Bimetallic Dendritic Nanoparticle: One-Step, High-Yield Synthesis and Its Bifunctional Plasmonic and Catalytic Properties. *J. Phys. Chem. C* **2010**, *114*, 15337–15342.
57. Hong, F.; Sun, S.; You, H.; Yang, S.; Fang, J.; Guo, S.; Yang, Z.; Ding, B.; Song, X. Cu_2O Template Strategy for the Synthesis of Structure-Definable Noble Metal Alloy Mesocages. *Cryst. Growth Des.* **2011**, *11*, 3694–3697.
58. Hong, J.; Kang, S. W.; Choi, B.; Kim, D.; Lee, S. B.; Han, S. W. Controlled Synthesis of Pd-Pt Alloy Hollow Nanostructures with Enhanced Catalytic Activities for Oxygen Reduction. *ACS Nano* **2012**, 10.1021/nn2046828.
59. Zhang, H.; Jin, M.; Liu, H.; Wang, J.; Kim, M. J.; Yang, D.; Xie, Z.; Liu, J.; Xia, Y. Facile Synthesis of Pd-Pt Alloy Nanocages and Their Enhanced Performance for Preferential Oxidation of CO in Excess Hydrogen. *ACS Nano* **2011**, *5*, 8212–8222.
60. Lu, X.; Chen, J.; Skrabalak, S. E.; Xia, Y. Galvanic Replacement Reaction: a Simple and Powerful Route to Hollow and Porous Metal Nanostructures. *Proc. Inst. Mech. Eng., Part N* **2007**, *221*, 1–16.
61. Waszkowiak, K.; Szymandera-Buszka, K. Effect of Storage Conditions on Potassium Iodide Stability in Iodised Table Salt and Collagen Preparations. *Int. J. Food Sci. Technol.* **2008**, *43*, 895–899.
62. Odugbemi, T.; Hafiz, S.; Mcentegart, M. Penicillinase-Producing Neisseria Gonorrhoeae: Detection by Starch Paper Technique. *Br. Med. J.* **1977**, *2*, 500–500.
63. Lu, C.; Prasad, S. K.; Wu, H.; Ho, J. A.; Huang, M. Au Nanocube-Directed Fabrication of Au−Pd Core−Shell Nanocrystals with Tetrahexahedral, Concave Octahedral, and Octahedral Structures and Their Electrocatalytic Activity. *J. Am. Chem. Soc.* **2010**, *132*, 14546–14553.
64. Yin, Y.; Erdonmez, C.; Aloni, S.; Alivisatos, P. Faceting of Nanocrystals during Chemical Transformation: From Solid Silver Spheres to Hollow Gold Octahedra. *J. Am. Chem. Soc.* **2006**, *128*, 12671–12673.
65. Zhang, Q.; Xie, J.; Lee, J. Y.; Zhang, J.; Boothroyd, C. Synthesis of Ag@AgAu Metal Core/Alloy Shell Bimetallic Nanoparticles with Tunable Shell Compositions by a Galvanic Replacement Reaction. *Small* **2008**, *4*, 1067–1071.
66. Mulvihill, M.; Ling, X.; Henzie, J.; Yang, P. Anisotropic Etching of Silver Nanoparticles for Plasmonic Structures Capable of Single-Particle SERS. *J. Am. Chem. Soc.* **2010**, *132*, 268–274.
67. Hong, J.; Lee, Y.; Kim, M.; Kang, S.; Han, S. One-Pot Synthesis and Electrocatalytic Activity of Octapodal Au−Pd Nanoparticles. *Chem. Commun.* **2011**, *47*, 2553–2555.

68. Xiong, Y. Morphological Changes in Ag Nanocrystals Triggered by Citrate Photoreduction and Governed by Oxidative Etching. *Chem. Commun.* **2011**, *47*, 1580–1582.
69. Cobley, C.; Rycenga, M.; Zhou, F.; Li, Z.; Xia, Y. Controlled Etching as a Route to High Quality Silver Nanospheres for Optical Studies. *J. Phys. Chem. C* **2009**, *113*, 16975–16982.
70. Min, M.; Kim, C.; Yang, Y.; Yi, J.; Lee, H. Top-Down Shaping of Metal Nanoparticles in Solution: Partially Etched Au@Pt Nanoparticles with Unique Morphology. *Chem. Commun.* **2011**, *47*, 8079–8081.
71. Lu, X.; Tu, H.; Chen, J.; Li, Z.; Korgel, B.; Xia, Y. Mechanistic Studies on the Galvanic Replacement Reaction between Multiply Twinned Particles of Ag and $HAuCl_4$ in an Organic Medium. *J. Am. Chem. Soc.* **2007**, *129*, 1733–1742.
72. Tao, A.; Habas, S.; Yang, P. Shape Control of Colloidal Metal Nanocrystals. *Small* **2008**, *4*, 310–325.
73. Cho, C.; Camargo, P. H. C.; Xia, Y. Synthesis and Characterization of Noble-Metal Nanostructures Containing Gold Nanorods in the Center. *Adv. Mater.* **2010**, *22*, 744–748.
74. Lou, Y.; Maye, M.; Han, L.; Luo, J.; Zhong, C. Gold-Platinum Alloy Nanoparticle Assembly as Catalyst for Methanol Electrooxidation. *Chem. Commun.* **2001**, 473–475.
75. Lu, X.; Au, L.; McLellan, J.; Li, Z.; Marquez, M.; Xia, Y. Fabrication of Cubic Nanocages and Nanoframes by Dealloying Au/Ag Alloy Nanoboxes with an Aqueous Etchant Based on $Fe(NO_3)_3$ or NH_4OH. *Nano Lett.* **2007**, *7*, 1764–1769.
76. Chang, C.; Wu, H.; Kuo, C.; Huang, M. Hydrothermal Synthesis of Monodispersed Octahedral Gold Nanocrystals with Five Different Size Ranges and Their Self-Assembled Structures. *Chem. Mater.* **2008**, *20*, 7570–7574.
77. Smith, D. K.; Miller, N. R.; Korgel, B. A. Iodide in CTAB Prevents Gold Nanorod Formation. *Langmuir* **2009**, *25*, 9518–9524.
78. Xiong, Y.; Cai, H.; Wiley, B. J.; Wang, J.; Kim, M. J.; Xia, Y. Synthesis and Mechanistic Study of Palladium Nanobars and Nanorods. *J. Am. Chem. Soc.* **2007**, *129*, 3665–3675.
79. Niu, W.; Zhang, L.; Xu, G. Shape-Controlled Synthesis of Single-Crystalline Palladium Nanocrystals. *ACS Nano* **2010**, *4*, 1987–1996.
80. Hoppe, C.; Lazzari, M.; Pardiñas-Blanco, I.; López-Quintela, M. One-Step Synthesis of Gold and Silver Hydrosols Using Poly(N-vinyl-2-pyrrolidone) as a Reducing Agent. *Langmuir* **2006**, *22*, 7027–7034.
81. Huang, X.; Zheng, N. One-Pot, High-Yield Synthesis of 5-Fold Twinned Pd Nanowires and Nanorods. *J. Am. Chem. Soc.* **2009**, *131*, 4602–4603.
82. Xiong, Y.; Washio, I.; Chen, J.; Cai, H.; Li, Z.; Xia, Y. Poly(vinyl pyrrolidone): A Dual Functional Reductant and Stabilizer for the Facile Synthesis of Noble Metal Nanoplates in Aqueous Solutions. *Langmuir* **2006**, *22*, 8563–8570.
83. Song, J.; Kim, F.; Kim, D.; Yang, P. Crystal Overgrowth on Gold Nanorods: Tuning the Shape, Facet, Aspect Ratio, and Composition of the Nanorods. *Chem.—Eur. J.* **2005**, *11*, 910–916.
84. Kim, Y.; Hong, J.; Lee, Y.; Kim, M.; Kim, D.; Yun, W.; Han, W. Synthesis of AuPt Heteronanostructures with Enhanced Electrocatalytic Activity toward Oxygen Reduction. *Angew. Chem., Int. Ed.* **2010**, *49*, 10197–10201.
85. Cheong, S.; Watt, J.; Ingham, B.; Toney, M.; Tilley, R. D. *In Situ* and *ex Situ* Studies of Platinum Nanocrystals: Growth and Evolution in Solution. *J. Am. Chem. Soc.* **2009**, *131*, 14590–14595.
86. Ah, C. S.; Yun, Y. J.; Park, H. J.; Kim, W.; Han, H. H.; Yun, W. S. Size-Controlled Synthesis of Machinable Single Crystalline Gold Nanoplates. *Chem. Mater.* **2005**, *17*, 5558–5561.
87. Carbó-Argiby, E.; Rodríguez-González, B.; Gómez-Graña, S.; Guerrero-Martínez, A.; Pastoriza-Santos, I.; Pérez-Juste, J.; Liz-Marzán, L. M. The Crystalline Structure of Gold Nanorods Revisited: Evidence for Higher-Index Lateral Facets. *Angew. Chem., Int. Ed.* **2010**, *49*, 9397–9400.
88. Sun, Y.; Xia, Y. Triangular Nanoplates of Silver: Synthesis, Characterization, and Use as Sacrificial Templates for Generating Triangular Nanorings of Gold. *Adv. Mater.* **2003**, *15*, 695–699.
89. Zhang, J.; Langille, M. R.; Personick, M. L.; Zhang, K.; Li, S.; Mirkin, C. A. Concave Cubic Gold Nanocrystals with High-Index Facets. *J. Am. Chem. Soc.* **2010**, *132*, 14012–14014.